Quantification of manganous ions in wine by NMR relaxometry

Philippe Bodart, Adam Rachocki, Jadwiga Tritt-Goc, Bernhard Michalke, Philippe Schmitt-Kopplin, Thomas Karbowiak, Régis Gougeon

Quantification of manganous ions in wine by NMR relaxometry.

Philippe R. Bodart[a,b,*], Adam Rachocki[c], Jadwiga Tritt-Goc[c], Bernhard Michalke[d], Philippe Schmitt-Kopplin[d,e] Thomas Karbowiak[a], and Regis D. Gougeon[a]

[a] Univ. Bourgogne Franche-Comté, Agrosup Dijon, UMR PAM A02.102, 1 Esplanade Erasme, 21000 Dijon, France.

[b] IUT A - Université des Sciences et Technologies de Lille, Villeneuve d'Ascq 59655, France.

[c] Institute of Molecular Physics, Polish Academy of Sciences, M. Smoluchowskiego 17, 60-179 Poznan, Poland.

[d] Research Unit Analytical BioGeoChemistry, Department of Environmental Sciences, Helmholtz Zentrum München, Ingolstaedter Landstrasse 1, 85764 Neuherberg, Germany.

[e] Chair of Analytical Food Chemistry, Technische Universität München, Alte Akademie 10, 85354 Freising-Weihenstephan, Germany.

Abstract

Proton relaxation in model and real wines is investigated for the first time by fast field cycling NMR relaxometry. The relaxation mechanism unambiguously originates form proton interaction with paramagnetic ions naturally present in wines. Profiles of a white Chardonnay wines from Burgundy, a red Medoc, and model wines are well reproduced by Solomon-Bloembergen-Morgan equations. Relaxation is primarily governed by interactions with Mn^{2+}. A straightforward model-independent quantification of the manganese ion concentration (down to few tens of µg/L) is proposed.

Keywords:

FFC NMR Relaxometry; wine; paramagnetic ions; manganese.

Introduction

Since the pioneering work of Eschnauer on trace elements [1,2], there has been a wealth of scientific publications tracing the various contributions throughout the overall winemaking process, from the vineyard to the ageing in bottles, which may have an impact on the transient concentrations of elements in grape and ultimately in wine [3–7]. Besides, multi-elemental fingerprinting has further proven to be a promising wine authentication strategy [8–10], although only recent studies have investigated the interplay between the winemaking processes and the viticultural origin of the grapes on the actual composition of wines [11]. Of all the elements present in wines, transition metals and in particular Fe and Cu have been the subject of many studies, since these two cations, with Mn to a lesser extent, were shown to play a central role in catalyzing oxidation [12,13]. Considered as natural elements in wine, whose presence is the result of a plant uptake from the soil [6], Fe, Cu, Mn, and also Ni, can be incorporated during winemaking, as a result of "contamination" from winery equipment or as a consequence of practices such as clarification and filtration [3,14]. Nevertheless, and despite the fact that the successive winemaking steps can modulate concentrations [5]; these four elements could be considered as discriminant among different Australian wine regions [15].

Although alternative methodologies such as Near Infrared Spectroscopy were proposed for the analysis of elements in wine [16], their quantification mostly relies on Atomic spectroscopy techniques, and in particular on inductively coupled plasma optical emission spectroscopy (ICP–OES), and mass spectrometry (ICP–MS). Many elemental analyses over the last decades have involved, and are still based on such techniques [9,17–20]. They can achieve very high selectivity and sensitivity, with reduced problems of interference due to matrix effects, but rely on expensive equipment. Furthermore, when dealing with biological samples like wine, metal speciation is a critical issue, and the association

of ICP-OES with fractionation strategies such as solid phase extraction has recently been used to discriminate Cu and Fe as hydrophobic, cationic and residual [13]. Besides, colorimetric or electrochemical methods have also been used for Cu and Fe speciation in wine [21].

To our knowledge, fast field cycling (FFC) NMR relaxometry has never been used to characterize wine and this preliminary communication aims to determine the origin of NMR relaxation in wine and to highlight some major information that could be extracted. FFC NMR relaxometry is the only low-field NMR technique that measures the longitudinal, or spin lattice relaxation time (T1), as a function of the magnetic field strength, over a wide range of frequencies (from a few kHz to tens of MHz) corresponding to values of T1 in the order of seconds to a fraction of a millisecond. Data are displayed in the form of a nuclear magnetic resonance dispersion (NMRD) profile, where the relaxation rate (R1 = 1/T1) is reported versus the Larmor frequency of the observed nuclei. Generally, the benefit of exploring the nuclear spin-lattice relaxation rate over a large range of frequencies is to isolate the typical NMRD features associated with different molecular dynamics. Varying the magnetic field (B_o) changes the Larmor frequency ($\nu_o = \gamma B_o/2\pi$, where γ is the gyromagnetic ratio of the observed nuclei) and therefore the time and length scales of the fluctuations responsible for the nuclear spin-lattice relaxation rate R1 [22–24]. It is possible to record NMRD profile of almost any material, solid, liquid, or colloid. In food science, FFC NMR has been applied to seeds[25], oil [26–28], fruits[29–31], cacao butter[32,33], starch[34], bread [35], honey [36,37], egg and meat [38–40], cheese[41], quality and anti-fraud controls [42]. The art of exploiting NMRD profile consists in finding a sensible model in the sense that it describes correctly the fluctuation of the NMR interactions, which requires a very good knowledge of the system studied which is for the less no obvious in many complex food systems.

Materials and methods

Field cycling NMR relaxometry.

Proton spin–lattice relaxation measurements were performed on a field cycling relaxometer from Stelar company (Mede, Italy) with a magnetic field B_o, covering the proton Larmor frequencies from 0.001 to 40 MHz [43–45]. The spectrometer operates by switching the current in a solenoidal magnet from a polarizing field (B_{pol}), corresponding to a proton Larmor frequency of 24 MHz, to a field of interest (B_{rel}) for a variable relaxation period (τ). After each τ delay, the B_{rel} field is switched to the acquisition field (B_{acqu}), corresponding to a proton Larmor frequency of 16 MHz, at which magnetization is detected after a π/2 pulse. The measurements were carried out at a temperature of 25°C, 4 scans were recorded, π/2 pulse was 10 µs, the field-switching time 3 ms, spectrometer dead time 18 µs, and spectral width 1.25 MHz. Points number 5 to 50 of fids were added to produce the relaxation curves, a single exponential relaxation curve was observed in each experiment and the decay/recovery curves at each B_{rel} value were fitted, using a single exponential function.

NMR titrations.

Metal titration curves were recorded at 25°C on a minispec mq20 (Bruker) operating at 19.65 MHz. Four scans were collected and experiments were repeated at least 4 times. Relaxation time T1 was measured with an inversion recovery pulse sequence. A single exponential relaxation curve was observed in each experiment.

Inductively coupled plasma atomic emission spectrometry.

An ICP-AES Spectro ARCOS system (SPECTRO Analytical Instruments GmbH & Co. KG, Kleve, Germany) was used for a complete screen of elements. The measured spectral element lines were: Cu:

324.754 nm, Fe: 259.941 nm, Mn: 257.611 nm, Mo: 202.030 nm, Ni: 231.614 nm. Sample introduction was carried out using a peristaltic pump connected to a Meinhard nebulizer with a cyclon spray chamber. The RF power was set to 1250 W, the plasma gas was 15 L Ar /min, whereas the nebuliser gas was 0.6 L Ar/min. After 1:20 dilution of the samples with Milli-Q H_2O for providing enough sample volume for measurements (only few µL had been available) they were directly analyzed. As a positive side effect the dilution eliminated probably occurring matrix effects and sensitivity changes due to ethanol from samples.

Samples.

A Chardonnay white wine (2014 vintage) from the University of Burgundy estate in Marsannay-la-Côte, Côte d'Or, France (samples W), and a red Medoc blend wine (2011 vintage) from Bordeaux (samples R) were selected for real wine analysis. A label (a or b) indicate that the experiment has been performed with the sample as received (Ra, Wa) or one year latter (Rb ,Wb). The Exchanged wine (EW) was produced by exchange of W on an acidic cation exchange resin: Dowex 50WX8-100 (capacity1.7 meq. mL^{-1}; Sigma–Aldrich), adapted from the procedure of Benitez [32]. The resin was activated with 10% HCl and washed with Milli-Q water until the eluate was neutral. Then, 20 mL W were mixed with 0.3 g of activated resin under stirring for 10 min. After filtration of the mixture on a 0.65 mm cellulose acetate membrane, the filtrate was stored at 4°C until analysis.

Ethanol (198.85 g, Aldrich ≥ 99.9%) was added to 1497.3 g of ultra-pure water with 7.5 g of citric acid to produce a 12% (vol) model wine. Anhydrous paramagnetic salts FeCl3 and $CuSO_4$ (Aldrich ≥ 99.99%), were used as received. $FeSO_4$.7H20 (Sigma ≥ 99.99) was also used as received, but the solute (water or hydro alcoholic solution) was degassed under N_2 down to an oxygen concentration of 0.5 mg/L) prior addition of the salt. $MnSO_4$.xH20 (Aldrich ≥ 99.99) was heated at 450°C during 14 hours to remove residual water [47,48]. $NiCl_3$.6H20 (Fluka >98.0%) was heated at 220°C for 10 hours to produce anhydrous chloride. Stock solutions of 50 mg/L of paramagnetic ions were diluted to obtain

targeted titration solutions. Laboratory glassware was cleaned three times with MilliQ water and ultrapure water prior syntheses of model wine used for the titration curves with Mn^{2+}, Ni^{2+}, Cu^{2+}, Fe^{2+}, and Fe^{3+}. The pH of model wines pH was 3.5, while white and red wine pH were 3.3 and 3.7 respectively. Samples are labelled MWx for Model Wine containing x/100 mg/L of manganese (i.e. MW005 contains 0.05mg/L of manganese).

Theoretical description

Any nucleus experiencing a space-dependent NMR interaction can generate a path for magnetic relaxation through the modulation of this interaction induced by nuclei dynamic. Modelling of relaxation profiles is not straightforward, and we only refer to the most simple and commonly-used models. In the case of proton NMR relaxometry of a solution, the first interaction to consider is the dipolar interaction between protons. At equilibrium, isolated ^1H nuclear spins placed in a magnetic field Bo occupy two energy levels $\pm h\nu_o/2$ whose population is given by the Boltzmann distribution [49] The unequal population of these two levels induces the Bo-proportional magnetization observed in NMR. In relaxation experiments, the sample, initially polarized in a strong external magnetic field (B_{pol}), is exposed to a lower relaxation magnetic field (B_{rel}), and the energy level populations are modified according to the second magnetic field. The magnetization has to relax in time, reaching eventually equilibrium at the lower field B_{rel} [23,50] The magnetization decay is generally exponential with a time constant referred to as the spin-lattice relaxation time T1. The simplest description of relaxation mechanisms results from the stochastic fluctuations of dipolar interactions between pairs of proton of the same molecule [49]. This intramolecular relaxation is associated with molecular rotation changing the orientation of the vector connecting the interacting nuclei (within a molecule) with respect to the direction of the external magnetic field (rotational diffusion model). The relaxation rate depends on the spectral density of this fluctuation and if Lorentzian spectral densities are considered it can be simply

expressed as the Bloembergen-Purcell-Pound (BPP) model. In the case of two identical spins it is written [24,51]:

$$\tilde{R}(\omega_I, \tau_o) = \tilde{C}_o \left[\frac{\tau_o}{1 + (\omega_I \tau_o)^2} + \frac{4\tau_o}{1 + 4(\omega_I \tau_o)^2} \right] \quad (1)$$

With:

$$\tilde{C}_o = \frac{3}{10} \left(\frac{\mu_o}{4\pi} \right)^2 \frac{{\gamma_I}^4 \hbar^2}{{r_{II}}^6} \quad (2)$$

Where ω_I is the Larmor pulsation of the observed nuclei (^{1}H), τ_o is the rotational correlation time, r_{II} is the distance between the two nuclei within the molecules, and the tilde accent specifies a two-spin interaction.

Paramagnetic relaxation is another, very efficient, relaxation mechanism resulting from the coupling between protons and unpaired electrons of any paramagnetic element. In particular, trace level of paramagnetic agents containing single ions are very effective relaxing agents in solution [52], and relaxometry has proven to be an efficient technique for various paramagnetic titrations [53–59].

Paramagnetic interactions are described by several mechanisms. The simplest one considers that the unpaired electrons are localized at the paramagnetic ion. The relaxation is described by an interaction between an electronic point dipole and a nuclear point dipole (Solomon mechanism).

The associated dipolar paramagnetic relaxation rate can be written in the case of two spins as [60–64]:

$$\tilde{R}_D(\omega_I, \tau_{d1}, \omega_s, \tau_{d2}) = \tilde{C}_D \left[\frac{7\tau_{d2}}{1 + (\omega_s \tau_{d2})^2} + \frac{3\tau_{d1}}{1 + (\omega_I \tau_{d1})^2} \right] \quad (3)$$

With

$$\tilde{C}_D = \frac{2}{15}\left(\frac{\mu_o}{4\pi}\right)^2 \frac{S(S+1)(\gamma_I\,\gamma_S\hbar)^2}{{r_{IS}}^6} \tag{4}$$

Where S is the electron spin number of the paramagnetic ion, and S-subscript refers to paramagnetic ion. Correlation time τ_{di} is a composition of the reorientational correlation time of the paramagnetic ion (τ_R) due to Brownian rotational motion, longitudinal (i=1) or transverse (i=2) electron relaxation time (τ_{Si}), and of the life time of the nuclei on the paramagnetic ion (τ_M):

$$\frac{1}{\tau_{di}} = \frac{1}{\tau_R} + \frac{1}{\tau_M} + \frac{1}{\tau_{Si}} \tag{5}$$

In practice, at low magnetic field, $\tau_{d1} = \tau_{d2} = \tau_d$ [65].

Equation (3) evidences two dispersions that can be observed at different frequencies. For certain aquaions, e.g. Cu^{2+} [62,64,66], Mn^{2+}[62,64,66,67], Fe^{3+}[62,64,68], Gd^{3+}[64,69], Cr^{3+} [62,65]) at room temperature and in low viscosity solutions, the first term in bracket of equation (3) is responsible for an inflection in the NMRD profile near 10 MHz ($\omega_s\tau_{d2}\sim1$) and arises essentially from τ_R [64]. But other aquaions do not show any dispersion below 40 MHz, e.g. Fe^{2+} [62], Co^{2+}[62], Ni2+[70]). Since $\omega_S = 658\omega_I$ [64], the second term ($\omega_I\tau_{d1}$) of equation (3), induces a dispersion at a significantly higher frequency, in the GigaHertz range (the same remark holds for equation (1)). The characterization and discrimination of these high frequency dispersions requires data collected at magnetic fields significantly higher than the 500 MHz frequency used in this study. It must be pointed out that these

considerations may be very different in other conditions (high viscosity, high temperature) or systems, (e.g. in macromolecules the $\omega_I \tau_{d1}$ dispersion may appear below 50 MHz [71–76]

[64] The Solomon mechanism is not always sufficient to reproduce the NMRD profiles. In particular, in the case of the paramagnetic nuclei present in wines, an additional fermi-contact interaction (Bloembergen mechanism) has to be considered. This interaction arises from a delocalization of the electronic wave function of the paramagnetic nuclei to the physical location of I-nuclei.

The relaxation rate in the case of two spins experiencing a contact interaction (scalar or hyperfine interaction) is given by [61–64]:

$$\tilde{R}_C(\omega_s, \tau_c) = \tilde{C}_C \left[\frac{\tau_c}{1 + (\omega_s \tau_c)^2}\right] \quad (6)$$

With:

$$\tilde{C}_C = \frac{2A^2 S(S+1)}{3\hbar^2} \quad (7)$$

Where A is the scalar coupling constant of the spin exchange interaction between nucleus and electron, and τ_c is given by:

$$\frac{1}{\tau_c} = \frac{1}{\tau_M} + \frac{1}{\tau_{S2}} \quad (8)$$

Several aquaions, (e.g. Fe^{3+}[62,68], Cr^{3+}[62,65] ,VO^{2+} [62,77]) experience this contact interaction, the associated dispersion in low viscosity solutions at room temperature is then situated at frequencies above 1 MHz. Manganous aquaions also experience a contact interaction with a characteristic low-field dispersive contribution (around 100 kHz) in the associated NMRD profile. Once more, in other conditions or systems, the previous consideration may be different.

Paramagnetic longitudinal relaxivity of the water protons (R_1^p) is given by [64,78]

$$\frac{pq}{R_1^p} = \frac{1}{\tilde{R}_D + \tilde{R}_C} + \tau_M \tag{9}$$

Where p is the concentration of the ions relative to the concentration of the solvent molecules (water) and q the number of metal-bound water molecules. Assuming a fast chemical exchange of the water molecules ($\tau_M \ll 1/(R_D + R_C)$. the relaxation of the water proton can be written:

$$R_1 = R + R_1^p = R + pq(\tilde{R}_C + \tilde{R}_D) = R + R_D + R_C \tag{10}$$

Where R can be associated to the background or solvent rate in the absence of paramagnetic ions, R_D and R_C are the dipolar and contact paramagnetic contribution from the exchange of solvent nuclei with the hydrated paramagnetic ions (first sphere of coordination). The contributions from second sphere and

longer range paramagnetic interactions are not considered here. When different types of solute paramagnetic ions are present, the contributions R_C and R_D of independent relaxation processes can be treated as additive [64], and (10) can be extended as:

$$R_1 = R + R_C^{Mn(II)} + \sum_{i \neq Mn} R_C^i + \sum_i R_D^i \quad (11)$$

Where i stands for all paramagnetic nuclei in the solution, $R_C^{Mn(II)}$ is explicitly reported to highlight the distinctive dispersion at ~0.1 MHz in wines at room temperature.

Detailed formalisms and more sophisticated developments can be found in reviews presenting theoretical description of paramagnetic NMR [52,63], but such developments are clearly beyond the scope of this communication.

Results and discussion

Wine NMRD profiles.

Beside NMRD profiles of model wines (MW samples), profiles of two distinct wines: a white Chardonnay from Burgundy (W samples) and a red Medoc blend (R samples) were also recorded. Samples were analyzed at two different times: as received in 2017 (Wa and Ra samples) and after one year exposed to atmospheric air in a closed NMR tube (ratio wine/air volume of 1/20; Wb and Rb samples). In wine, naturally present paramagnetic ions have low (mg/L) or very low (µg/L) concentrations, typical orders rarely exceed 5 mg/L for iron, 2 mg/L for manganese and are less than 1mg/L for copper [5]. ICP-AES analyses of our samples are reported in Table 1.

Table 1. *Concentrations (mg/L) of paramagnetic elements measured in the white Chardonnay (W), the red Medoc (R) and the exchanged wine (EW) by ICP-AES. Numbers in parentheses are the uncertainties on the last digits.*

	Mn	Fe	Cu	Ni	Cd
W	1.26(2)	1.34(2)	0.160(2)	0.91(1)	0.0019(1)
EW	<0,002	0.056(3)	0.024(1)	<0,007	<0,001
R	1.06(2)	0.85(1)	0.93(1)	0.065(1)	0.0056(3)

To test paramagnetic relaxation mechanism in wine, Fig. 1 reports NMRD profiles of the white wine recorded before (Wa) and after (EW) ion exchange treatment on a resin to remove paramagnetic ions [46]. When paramagnetic ions are extracted from the wine, a featureless profile with longer relaxation times is observed, confirming the dominant paramagnetic relaxation mechanisms in wine. Moreover, in Wa profile, the low frequency dispersion around 0.1 MHz is characteristic of manganese, and in a first approximation proton coupling with manganese has to be assumed. For comparison, the NMRD profiles of two model wines (MW005 and MW128) solely containing manganese as paramagnetic ions at levels of 50 µg/L and 1.28 mg/L and the profile of the red wine are reported in Fig. 1.

Fig. 1.

The shapes of the real and model wine profiles are similar. Furthermore, the clear manganese fingerprint characterized by two dispersions around 0.1 and 10 MHz observed in MW005, indicates that 50µg/L is clearly above the limit of detection and quantification. In Fig. 1, NMRD profiles of Wa and model wines are satisfactory reproduced with the following equation:

$$R_1 = R(\omega_I, \tau_o) + R_D(\omega_I, \omega_s, \tau_d) + R_C(\omega_s, \tau_c) \quad (12)$$

Numerical parameters resulting from the refinement are gathered in Table 2 with additional results of wines and model wines containing 5.43 (MW543), 5.01 (MW501), and 0.53 (MW053) mg/L of Mn^{2+}. Since we do not have high frequency data to refine the diamagnetic contribution (equation (1), the relaxation rate of the model wine without paramagnetic elements measured at 20 MHz (0.47 s^{-1}) was used to fix the diamagnetic contribution ($R(\omega_I, \tau_o)$).

Table 2. *Parameters obtained from refinements of NMRD profiles for the white Chardonnay (W), the red Medoc blend (R) and model wines (MW). MWx refers to model wines containing x/100 mg/L of manganese. .* $C_{D/C} = pq\tilde{C}_{D/C}$ *and Numbers in parentheses are last-digit-uncertainties resulting purely from the numerical refinement.*

	R_D		R_C	
	C_D (10^9 s^{-2})	τ_d (10^{-11}s)	C_C (10^9 s^{-2})	τ_c (10^{-9} s)
MW546	5.78	3.81(2)	1.41	1.88(1)
MW501	5.47	3.78(2)	1.27	1.86(2)
MW128	1.64	3.60(3)	0.34	1.87(3)
MW053	0.72	3.43(3)	0.14	1.82(3)
MW005	0.25	1.80(2)	0.02	1.50(4)
Wa	2.73	2.82(3)	0.33	1.51(3)
Wb	2.69	2.92(2)	0.36	1.43(2)
Ra	2.97	2.56(2)	0.30	1.28(3)
Rb	2.07	3.22(3)	0.30	1.38(4)

. In Table 2, correlation times τ_d and τ_c are consistent with literature data of Mn^{2+} in solution [64,62,67,77,79]. Among model wine samples, little deviations are observed, the somehow lower correlation times measured for MW005 may simply result from the noisier data. However, the measured dipolar values differ notably between the two red wines. In fact, an inspection of samples Ra and Rb revealed that, while Ra has a natural red color, Rb turned very brown indicating a contact with air. This air-contact, among various changes in the wine, induces oxidation and eventually evaporation of alcohol, which contribute to a decrease of the relaxation rate (Fig. 4.). The signature of this oxidation is already observable on Ra and Rb profiles (Fig. 1.c), Rb curve is downward-shifted with respect to Ra one (~0.1 s^{-1}at 20 MHz). The refinement of the Rb profile is performed with a diamagnetic contribution fixed to 0.47 s^{-1} which is of course unappropriated in the case of Rb and the 0.1s^{-1} shift is numerically reported in the C_D parameter.

Variation of parameters C_D and C_C versus the manganese concentration for the model wines is reported in Fig. 2.

Fig. 2

The C_C parameter results from the contact interaction proper to Mn^{2+}, therefore a report of C_C obtained from Wa NMRD profile, on the line of Fig. 2 gives a measure of the manganese concentration in the wine: 1.26±0.08 mg/L. . Results obtained for other samples are reported in Table 3, the relaxation measurement of the manganese concentration agrees (within incertitude limits) with the ICP-AES analysis, confirming the major role of manganese in the paramagnetic relaxation mechanism

Table 3. *Manganese concentrations (mg/L) in wine samples measured by ICP-AES and relaxometry. Concentrations reported in column C are calculated through the contact constant of the Solomon-Bloembergen-Morgan equation. Numbers in parentheses are uncertainties on the last digits.*

	ICP-AES	C
Wa	1.26(2)	1.26(8)
Wb		1.38(8)
Ra	1.06(2)	1.15(8)
Rb		1.13(8)

The dispersion around 10 MHz can be affected by the dipolar or contact interactions of other paramagnetic present in the wine (Fe[66,62], Cu[62]) and the report of C_D on Fig. 2 can overestimate the Mn^{2+} concentration. Dispersions of other paramagnetic nuclei is also the probable explanation for the mismatch of the simulated profile and the experimental points around 10 MHz. Furthermore, it may as well contribute to the difference observed around 10 MHz between the profiles of model wine MW128 and Wa, which have very close Mn^{2+} concentrations and should match once vertically shifted (Fig. 1.a). Since the wines contain several paramagnetic elements (Table 1), it is important to examine how other paramagnetic nuclei could contribute to the relaxation of the wine, and be observed in the NMRD profiles.

Fig. 3

Fig. 3 reports the relaxation rates recorded at a Larmor frequency of 19.65 MHz measured on model wines containing variable amount of paramagnetic nuclei present in the wines (Cu^{2+},Fe^{2+}, Mn^{2+}, Ni^{2+},

Fe^{3+}). Intercepts, and slopes (the proton relaxivities) of the linear correlations and some related literature values are reported in Table 4.

Table 4. *Proton relaxivity (r) and intercept (*R_0*) of model wines and water solutions containing metal ions (Mn^{2+}, Fe^{3+}, Fe^{2+}, Ni^{2+} and Cu^{2+}). If not specified otherwise, measurements were performed at 19.65 MHz and at 25°C. Numbers in parenthesis indicate last-digit-uncertainties.* [a]*$MnCl_2$ N_2-degassed solution at 37°C*[80]. [b] *$Fe(NO_3)_3$ in 1M $HCL0_4$*[68]. [c]*$FeCl_3$.6H20 solution, at 22°C, pH=1, ν_{Larmor} =9.1MHz* [81]. [d]*$FeCl_3$ or $Fe(NO_3)_3$, in 1.4M HCl (*) or 5%HNO_3 (**), ν_{Larmor} =60 MHz* [58]. [e]*$CuSO_4$ solution* [82]. [f] *from a NMRD profile* [62]. [g] *from Figure 6 of Schlüter* [55]. [h] $Ni(ClO_4)_2$ solution, pH 0.1-3, ν_{Larmor} *=12 MHz*[83,84]. [i]*$(NH_4)_2Fe(SO_4)_2$ solution at 37°C, pH=1*[85]. [j]*measured on fresh $FeSO_4.7H_2O$ solution, in N2 degassed water (~ 0.5mg/L of O_2)*[86]. [k] *from a NMRD profile of a 10mM of $(NH_4)_2Fe(SO_4)_2$*[62].

	R_0 (wine) (s^{-1})	r (wine) s^{-1} $(mg/L)^{-1}$	r (H_2O solution) s^{-1} $(mg/L)^{-1}$
Mn^{2+}	0.467(3)	0.155(1)	0.126[a]
Fe^{3+}	0.441(8) 0.477(3)	0.092(4) 0.065(1)	0.21[b]; 0.1792(4)[c]; 0.012*,0.019**[d]
Cu^{2+}	0.4591(3)	0.0140(2)	0.02[e]; 0.014[f]
Ni^{2+}	0.4867(4)	0.0065(1)	0.015[g]; 0.010[h]
Fe^{2+}	0.47(1)	0.0075(5)	0.008[i]; 0.0065[j]; 0.0067[k]

Comparable linear correlations have been reported for T1 and T2 relaxations for various paramagnetic ions in solution [57,58,80,82,87]. The curves intercept the y-axis at a value, which would be the relaxation rate of the model wine free of paramagnetic element (R_0), which can thus be considered as

the solvent relaxation rate. Relaxivities of Fe^{2+}, Ni^{2+}, and Cu^{2+} ions are at least one order of magnitude inferior to the Mn^{2+} one and are not expected to significantly participate to the dipolar dispersion. Ferric aquaion which has a dispersive component around 7 MHz[62,68] is the only candidate that could contribute to the dipolar paramagnetic relaxation. This is a very interesting point that relaxometry could highlight in situ. Indeed iron plays a determinant catalytic role in oxidation mechanism of wine. However, because of the tens of thousands of molecules and elements present in wine, oxidation mechanisms are very complex and have been the subject of numerous works [88–95]. It is well known that when wine is preserved from oxygen, iron is preferably in ferrous state and should therefore not contribute significantly to the relaxation. However, in the presence of O_2, it is oxidized to Fe^{3+} and it has been shown in real wines that Fe^{2+} concentration can decrease by 40 – 50 % in 80 hours after exposure to air[96]. Fe^{3+} is very likely to occur in our samples and increase the observed dispersion at 10 MHz. When oxidation processes are completed, Fe^{3+} can be reduced or form complexes and insoluble particles (i.e. $Fe(OH)_3$) that contribute to a lesser extent to the relaxation [54,56,59]. . ICP-AES analysis of exchanged wine (EW), has revealed Mn^{2+}concentration below 0.002 mg/L. In Fig. 1, the NMR profile of EW shows a barely visible decreasing slope of the relaxation rate but no clear manganese signature is visible. A few µg/L of Mn^{2+} would be the limit of detection, at least within our experimental conditions. It is worth noting that in other systems (such as wine vinegars), profiles may show different paramagnetic signatures as a hump at high frequency [42,52,63,75], which results from the formation of big-size paramagnetic complexes (with sugars or organic acids), which is not observed in wine.

Manganese titration in wines.

In the following, we propose a method to quantify the manganese concentration in wines, in a simple model free approach. This is of interest for wine control or identification. The goal is to remove

miscalculation due to other paramagnetic ions like Fe^{3+} but also R_0-contribution that, for many reasons, may vary from one wine to another. As an illustration of such effects is presented in Fig. 4 where the relaxation rate of different model wines are reported versus the alcoholic strength of the solutions. It is worth noting that the linear dependence over the alcohol percent is no longer verified above ~40 % in volume of alcohol [97].

Fig. 4.

Variation of the synthetic wine relaxivity versus Mn^{2+} concentration for various Larmor frequencies is reported in Fig.1S in the supplementary information. A linear dependence is confirmed for all frequencies and can be simply formalized as:

$$R_{\nu A} = b_{\nu A} + r_{\nu A}^{Mn} \, . C^{Mn} \tag{13}$$

Where $R_{\nu A}$ stands for the relaxation rate at a Larmor frequency νA, $r_{\nu A}^{Mn}$, and $b_{\nu A}$ are the relaxivity and the intercept at νA, and C^{Mn} is the concentration of Mn^{2+}. The intercept (0.51 s^{-1}) shows little variations (±0.02 s^{-1}), and it is convenient to assume it independent of the Larmor frequency and to associate it with the relaxation rate of the solvent R_0 when no manganese is present in the wine [52].

Equation (13) can be written as:

$$R_{\nu A} = R_0 + r_{\nu A}^{Mn} . C^{Mn} \tag{14}$$

Considering two points A and B on the wine profile we may extract the manganese concentration according to:

$$C^{Mn} = \frac{R_{\nu A} - R_{\nu B}}{r_{\nu A}^{Mn} - r_{\nu B}^{Mn}} \tag{15}$$

Equation (15) is in principle valid for any couple of frequency, and does only depend on the slopes of the titration lines at frequencies A and B. In particular, if we consider two points below roughly 1MHz, and since R_D can reasonably be approximated to a constant value (Fig. 1) any dipolar contribution is cancelled in the numerator of equation (15) and this equation only quantifies the manganese involved in the contact interaction. All possible significant paramagnetic contributions from other nuclei (Cu^{2+}, Fe^{2+}, Fe^{3+}, Ni^{2+}) vanish. Moreover, by the same way, equation (15) does also eliminate the solvent contribution (R or R_0 in equation (1) or (14)), i.e. it is independent of chemical or physical properties that may give different intercepts from one wine to another. Consequently, equation (15) should allow for a straightforward and robust estimation of the manganese concentration within the samples. Fig. 5 illustrates the calculation for all possible frequency couples for a model wine containing 0.53mg/L of Mn^{2+} (MW053).

Fig. 5

Two areas of the contour plot give unsatisfactory results: (i) the diagonal zone for which two close frequencies are chosen and unsurprisingly the reliability decreases as frequencies come closer, (ii) a low frequency band (<0.02 MHz) for which the collected data are less reliable due to imperfect magnetic earth field compensation during the measurement. Couples of point taken from the two plateaus of the NMRD profile (in the ranges 0.02-0.06 and 1-3 MHz) are expected to give good results since relaxation rates are significantly different between the two ranges, whereas within each zone, the variation is smooth. This area corresponds to the square in Fig. 5, and is approximately situated in the middle of the grey area where all calculated concentrations are in the range 0.53 ± 0.02 mg/L. Indeed, the manganese concentration calculated with the 25 points in the square is 0.53 ±0.01 mg/L, in good agreement with the expected value of 0.53 mg/L. Even when the calculation zone extends to the dashed rectangle (120

points) and the triangle (300 points), concentrations are stable: 0.52 ±0.01 and 0.53 ±0.05 mg/L, respectively. Comparable results are obtained for all other model wines (Table 5).

Table 5. *Calculated manganese concentration (mg/L) according to equation (15). In the square zone, 25 points are used for the statistical calculation, 120 and 300 points are considered in the rectangle and triangle zone, respectively. Samples Wa and Ra are recorded with different experimental condition but approximately the same zones have been chosen however, only 12, 72 and 171 experimental points are in the zones. Numbers in parenthesis indicate the standard deviation on the last digit.* [a] *Concentration measured by ICP AES*

	Manganese concentration	Square zone	Rectangular zone	Triangular zone
MW546	5.46	5.46(3)	5.45 (4)	5.5 (1)
MW501	5.01	4.97(5)	4.97(6)	5.0(1)
MW128	1.28	1.34(8)	1.3(1)	1.3 (1)
MW053	0.53	0.53(1)	0.52 (1)	0.53 (5)
MW005	0.05	0.063(5)	0.063 (6)	0.06 (1)
Wa	1.26(2)[a]	1.17(9)	1.2(1)	1.3(2)
Wb		1.13(3)	1.1(1)	1.4(2)
EW	<0.002[a]	0.009(6)	0.011(4)	0.01 (1)
Ra	1.06(2)[a]	0.83(4)	0.9(1)	1.2(3)
Rb		0.91(5)	0.9(1)	1.2(3)

Fig. 6.

The concentration contour plot of Wa is reported in Fig. 6, and presents similarities with Fig. 5. Low and diagonal frequencies are subject to more variation but the calculated concentrations are more

dispersed, in particular for the higher frequencies of the triangular zone, and the plateau supporting the rectangular zone is not so well defined: concentrations are monotonously increasing along the x-axis. From square to triangle, the concentrations are calculated to be 1.17 ±0.09, 1.2 ±0.1 and 1.3 ±0.2 mg/L (Table 5), in very good agreement with the calculated concentration issued from the refinement of the low field dispersion.

While in the case of model wines, the three calculated concentrations were fairly consistent, for the real wines some variations are observed, particularly in the upper part of the triangle zone. We may attribute this deviation to the additional paramagnetic elements present in the wine. Even though other paramagnetic ions have a low relaxivity with respect to Mn^{2+} (Fig. 3), when couples of high frequencies are considered, the profile is mainly governed by the dipolar dispersion, and the cumulative dipolar contributions of other paramagnetic ions (Fe^{3+}, Cu^{2+},Ni^{2+}) may then be less negligible and result in an increase of the calculated manganese concentration. If one wishes to further analyze the results, it appears that the concentrations are slightly underestimated. This could be explained by the fact that on NMRD profiles, manganese complexation is particularly visible on the low field dispersion caused by the contact interaction, which induces a decrease of the relaxation rate [54,79]. Since wine has a high tendency for forming complexes with minor and trace-metal cations [5,17,98,99], we could attribute the manganese concentration deficit observed on the low field singularity to the complexation of Mn^{2+}. On overall, while manganese concentration is measured with very high accuracy on model wine, small differences remain between ICP-AES and relaxometric measurement performed on real wines. NMRD profiles may still contain unrevealed information.

Despite no manganese signature on the NMRD profile of the exchanged wine is visible, equation (15) is also applied to the exchanged wine sample, and reasonable concentrations of the order of 0.01 mg/L are obtained (ICP-AES analysis gives less than 0.002 mg/L (Table 5)).

Conclusions

NMR proton relaxation of wine clearly originates from paramagnetic ions naturally present in wine. In the samples studied the relaxation is governed by Mn^{2+} relaxation for which very low concentration (few tens of µg/L) can be quantify in situ with a good accuracy. Moreover, NMR relaxometry should also be able to reveal Fe^{3+} when present. The double dispersion signature of Mn^{2+} observed on proton profile allows in a model independent straightforward calculation for a simple and precise measurement of manganese concentration independently of all other paramagnetic ions, or solvent effect and could reveal manganese complexation. This approach is obviously not limited to wine and should be usable for various chemical solution, biological fluids, or gels.

Author information

Corresponding Author

* Philippe.bodart@u-bourgogne.fr

Author Contributions

The manuscript was written through contributions of all authors. All authors have given approval to the final version of the manuscript. P.R.B. and A.R. performed the NMR experiments. |B.M. performed the ICP analyses. J.T-G, R.D.G., T.K., and P.S-K. contributed to materials and analysis tools. P.R.B. and R.D.G wrote the communication.

Notes

The authors declare no competing financial interest.

Acknowledgements

Authors are grateful to COST Action CA15209 European Network on NMR Relaxometry (EURELAX)

P.R.B. thanks Aymerick Batlogg for synthesizing and T1 measurements at 19.65 MHz of Fe-model wines as well as for the data of Figure 4. Authors are very thankful to the referees for their valuable comments. This work was supported by the regional council of Bourgogne Franche comté and the "Fonds Européen de Développement Régional (FEDER)". Graphical Abstract based on a design by rawpixel.com / Freepik.

REFERENCES

[1] H. Eschnauer, Spurenelemente in Wein und anderen Getrinken., Weinheim, 1974.
[2] H. Eschnauer, Trace Elements in Must and Wine: Primary and Secondary Contents, Am. J. Enol. Vitic. 33 (1982) 226.
[3] C.M.R. Almeida, M.T.S.D. Vasconcelos, Multielement Composition of Wines and Their Precursors Including Provenance Soil and Their Potentialities As Fingerprints of Wine Origin, Journal of Agricultural and Food Chemistry. 51 (2003) 4788–4798. https://doi.org/10.1021/jf034145b.
[4] G. Nicolini, R. Larcher, P. Pangrazzi, L. Bontempo, Changes in the contents of micro- and trace-elements in wine due to winemaking treatments, Vitis. 43 (2004) 41–45.
[5] P. Pohl, What do metals tell us about wine?, TrAC Trends in Analytical Chemistry. 26 (2007) 941–949. https://doi.org/10.1016/j.trac.2007.07.005.
[6] M.G. Volpe, F. La Cara, F. Volpe, A. De Mattia, V. Serino, F. Petitto, C. Zavalloni, F. Limone, R. Pellecchia, P.P. De Prisco, M. Di Stasio, Heavy metal uptake in the enological food chain, Food Chemistry. 117 (2009) 553–560. https://doi.org/10.1016/j.foodchem.2009.04.033.
[7] H. Hopfer, J. Nelson, A.E. Mitchell, H. Heymann, S.E. Ebeler, Profiling the trace metal composition of wine as a function of storage temperature and packaging type, Journal of Analytical Atomic Spectrometry. 28 (2013) 1288–1291. https://doi.org/10.1039/c3ja50098e.
[8] J.D. Greenough, H.P. Longerich, S.E. Jackson, Element fingerprinting of Okanagan Valley wines using ICP-MS: Relationships between wine composition, vineyard and wine colour, Australian Journal of Grape and Wine Research. 3 (1997) 75–83. https://doi.org/10.1111/j.1755-0238.1997.tb00118.x.
[9] M. J. Baxter, H. M. Crews, M. John Dennis, I. Goodall, D. Anderson, The determination of the authenticity of wine from its trace element composition, Food Chemistry. 60 (1997) 443–450. https://doi.org/10.1016/S0308-8146(96)00365-2.
[10] P.P. Coetzee, F.E. Steffens, R.J. Eiselen, O.P. Augustyn, L. Balcaen, F. Vanhaecke, Multi-element Analysis of South African Wines by ICP–MS and Their Classification According to Geographical Origin, Journal of Agricultural and Food Chemistry. 53 (2005) 5060–5066. https://doi.org/10.1021/jf048268n.

[11] H. Hopfer, J. Nelson, T.S. Collins, H. Heymann, S.E. Ebeler, The combined impact of vineyard origin and processing winery on the elemental profile of red wines, Food Chemistry. 172 (2015) 486–496. https://doi.org/10.1016/j.foodchem.2014.09.113.
[12] J.C. Danilewicz, Fe(II):Fe(III) Ratio and Redox Status of White Wines, American Journal of Enology and Viticulture. 67 (2016) 146–152. https://doi.org/10.5344/ajev.2015.15088.
[13] M. Rousseva, N. Kontoudakis, L.M. Schmidtke, G.R. Scollary, A.C. Clark, Impact of wine production on the fractionation of copper and iron in Chardonnay wine: Implications for oxygen consumption, Food Chemistry. 203 (2016) 440–447. https://doi.org/10.1016/j.foodchem.2016.02.081.
[14] H. Eschnauer, L. Jakob, H. Meierer, R. Neeb, Use and limitations of ICP-OES in wine analysis, Microchimica Acta. 99 (1989) 291–298. https://doi.org/10.1007/BF01244684.
[15] A.E. Martin, R.J. Watling, G.S. Lee, The multi-element determination and regional discrimination of Australian wines, Food Chemistry. 133 (2012) 1081–1089. https://doi.org/10.1016/j.foodchem.2012.02.013.
[16] D. Cozzolino, M.J. Kwiatkowski, R.G. Dambergs, W.U. Cynkar, L.J. Janik, G. Skouroumounis, M. Gishen, Analysis of elements in wine using near infrared spectroscopy and partial least squares regression, Talanta. 74 (2008) 711–716. https://doi.org/10.1016/j.talanta.2007.06.045.
[17] M. Latorre, P. Herbello-Hermelo, C. Peña-Farfal, Y. Neira, P. Bermejo-Barrera, A. Moreda-Piñeiro, Size exclusion chromatography – Inductively coupled plasma – Mass spectrometry for determining metal-low molecular weight compound complexes in natural wines, Talanta. 195 (2019) 558–565. https://doi.org/10.1016/j.talanta.2018.11.055.
[18] S. Kelly, K. Heaton, J. Hoogewerff, Tracing the geographical origin of food: The application of multi-element and multi-isotope analysis, Trends in Food Science & Technology. 16 (2005) 555–567. https://doi.org/10.1016/j.tifs.2005.08.008.
[19] S.A. Drivelos, C.A. Georgiou, Multi-element and multi-isotope-ratio analysis to determine the geographical origin of foods in the European Union, TrAC Trends in Analytical Chemistry. 40 (2012) 38–51. https://doi.org/10.1016/j.trac.2012.08.003.
[20] E.P. Pérez-Álvarez, R. Garcia, P. Barrulas, C. Dias, M.J. Cabrita, T. Garde-Cerdán, Classification of wines according to several factors by ICP-MS multi-element analysis, Food Chemistry. 270 (2019) 273–280. https://doi.org/10.1016/j.foodchem.2018.07.087.
[21] N. Kontoudakis, L.M. Schmidtke, M.Z. Bekker, M. Smith, P.A. Smith, G.R. Scollary, E.N. Wilkes, A.C. Clark, Analytical strategies for the measurement of different forms of Cu and Fe in wine: Comparison between approaches in relation to wine composition, Food Chemistry. 274 (2019) 89–99. https://doi.org/10.1016/j.foodchem.2018.08.084.
[22] D. Kruk, Theory of evolution and relaxation of multi-spin systems: application to nuclear magnetic resonance and electron spin resonance, arima publ, Bury St Edmunds, 2007.
[23] R. Kimmich, NMR Tomography, Diffusometry, Relaxometry, Springer Berlin, Berlin, 2013.
[24] D. Kruk, Understanding spin dynamics, Pan Stanford Publishing, Singapore, 2016.
[25] A. Rachocki, L. Latanowicz, J. Tritt-Goc, Dynamic processes and chemical composition of Lepidium sativum seeds determined by means of field-cycling NMR relaxometry and NMR spectroscopy, Anal Bioanal Chem. 404 (2012) 3155–3164. https://doi.org/10.1007/s00216-012-6409-5.
[26] A. Rachocki, J. Tritt-Goc, Novel application of NMR relaxometry in studies of diffusion in virgin rape oil, Food Chemistry. 152 (2014) 94–99. https://doi.org/10.1016/j.foodchem.2013.11.112.
[27] P. Conte, V. Mineo, S. Bubici, C. De Pasquale, F. Aboud, A. Maccotta, D. Planeta, G. Alonzo, Dynamics of pistachio oils by proton nuclear magnetic resonance relaxation dispersion, Anal Bioanal Chem. 400 (2011) 1443–1450. https://doi.org/10.1007/s00216-011-4904-8.

[28] P. Conte, A. Maccotta, C.D. Pasquale, G. Alonzo, Supramolecular organization of triglycerides in extra-virgin olive oils as assessed by nmr relaxometry, Fresenius Environmental Bulletin. 19 (2010) 6.
[29] P. Conte, S. Bubici, E. Palazzolo, G. Alonzo, Solid-State ^{1}H-NMR Relaxation Properties of the Fruit of a Wild Relative of Eggplant at Different Proton Larmor Frequencies, Spectroscopy Letters. 42 (2009) 235–239. https://doi.org/10.1080/00387010902895038.
[30] R. Lo Scalzo, M. Fibiani, G. Francese, A. D'Alessandro, G.L. Rotino, P. Conte, G. Mennella, Cooking influence on physico-chemical fruit characteristics of eggplant (Solanum melongena L.), Food Chemistry. 194 (2016) 835–842. https://doi.org/10.1016/j.foodchem.2015.08.063.
[31] D. Capitani, A.P. Sobolev, M. Delfini, S. Vista, R. Antiochia, N. Proietti, S. Bubici, G. Ferrante, S. Carradori, F.R.D. Salvador, L. Mannina, NMR methodologies in the analysis of blueberries: General, ELECTROPHORESIS. 35 (2014) 1615–1626. https://doi.org/10.1002/elps.201300629.
[32] M. Ladd-Parada, M.J. Povey, J. Vieira, M.E. Ries, Fast field cycling NMR relaxometry studies of molten and cooled cocoa butter, Molecular Physics. 117 (2019) 1020–1027. https://doi.org/10.1080/00268976.2018.1508784.
[33] M. Ladd Parada, M.J. Povey, J. Vieira, M. Rappolt, M.E. Ries, Early stages of fat crystallisation evaluated by low-field NMR and small-angle X-ray scattering, Magn Reson Chem. (2019). https://doi.org/10.1002/mrc.4860.
[34] M.I.B. Tavares, E.O. da Silva, P.S.R.C. Silva, P.J. Sebastião, The use of fast field cycling to evaluate the time domain relaxation of starches from tropical fruit seeds, Molecular Physics. 117 (2019) 1028–1033. https://doi.org/10.1080/00268976.2018.1540803.
[35] E. Curti, S. Bubici, E. Carini, S. Baroni, E. Vittadini, Water molecular dynamics during bread staling by Nuclear Magnetic Resonance, LWT - Food Science and Technology. 44 (2011) 854–859. https://doi.org/10.1016/j.lwt.2010.11.021.
[36] G. Cimo', P. Conte, Conformational Redistribution of Honey Components following Different Storage Conditions, International Journal of Spectroscopy. 2015 (2015) 1–7. https://doi.org/10.1155/2015/354327.
[37] I. Płowaś-Korus, Ł. Masewicz, A. Szwengiel, A. Rachocki, H.M. Baranowska, W. Medycki, A novel method of recognizing liquefied honey, Food Chemistry. 245 (2018) 885–889. https://doi.org/10.1016/j.foodchem.2017.11.087.
[38] L. Laghi, M.A. Cremonini, G. Placucci, S. Sykora, K. Wright, B. Hills, A proton NMR relaxation study of hen egg quality, Magnetic Resonance Imaging. 23 (2005) 501–510. https://doi.org/10.1016/j.mri.2004.12.003.
[39] F. Bajd, A. Gradišek, T. Apih, I. Serša, Dry-cured ham tissue characterization by fast field cycling NMR relaxometry and quantitative magnetization transfer: FFC/qMT-NMR study of dry-cured hams, Magn. Reson. Chem. 54 (2016) 827–834. https://doi.org/10.1002/mrc.4462.
[40] S.S. Uguz, E.B. Ozvural, M.J. Beira, M.H. Oztop, P.J. Sebastião, Use of NMR Relaxometry to identify frankfurters of different meat sources, Molecular Physics. 117 (2019) 1015–1019. https://doi.org/10.1080/00268976.2018.1542162.
[41] S. Godefroy, J.-P. Korb, L.K. Creamer, P.J. Watkinson, P.T. Callaghan, Probing protein hydration and aging of food materials by the magnetic field dependence of proton spin-lattice relaxation times, Journal of Colloid and Interface Science. 267 (2003) 337–342. https://doi.org/10.1016/S0021-9797(03)00589-7.
[42] S. Baroni, R. Consonni, G. Ferrante, S. Aime, Relaxometric Studies for Food Characterization: The Case of Balsamic and Traditional Balsamic Vinegars, Journal of Agricultural and Food Chemistry. 57 (2009) 3028–3032. https://doi.org/10.1021/jf803727d.
[43] E. Anoardo, G. Galli, G. Ferrante, Fast-field-cycling NMR: applications and instrumentation, Applied Magnetic Resonance. 20 (2001) 365–404.

[44] R. Kimmich, E. Anoardo, Field-cycling NMR relaxometry, Progress in Nuclear Magnetic Resonance Spectroscopy. 44 (2004) 257–320. https://doi.org/10.1016/j.pnmrs.2004.03.002.
[45] F. Noack, NMR field-cycling spectroscopy: principles and aplications, Progress in Nuclear Magnetic Resonance Spectroscopy. 18 (1986) 171–276. https://doi.org/10.1016/0079-6565(86)80004-8.
[46] P. Benítez, R. Castro, C.G. Barroso, Removal of iron, copper and manganese from white wines through ion exchange techniques: effects on their organoleptic characteristics and susceptibility to browning, Analytica Chimica Acta. 458 (2002) 197–202. https://doi.org/10.1016/S0003-2670(01)01499-4.
[47] J.H. Krepelka, B. Rejha, The anhydrous and the hydrated manganous sulphates.- part I, Collect. Czech. Chem. Commun. 3 (1931) 517–535.
[48] S.G. Sinha, N.D. Deshpande, D.A. Deshpande, Dehydratation of crystalline MnSO4.4H2O, Thermochimica Acta. 113 (1987) 95–104.
[49] A. Abragam, The principles of nuclear magnetism, Reprinted, Oxford Univ. Press, Oxford, 2006.
[50] R. Kimmich, Field Cycling in NMR Relaxation Spectroscopy: Applications in Biological, Chemical and Polymer Physics, Bull. magn reson. 1 (1980) 24.
[51] N. Bloembergen, E.M. Purcell, R.V. Pound, Relaxation effects in nuclear magnetic resonance absorption, Physical Review. 73 (1948) 679–712.
[52] S.H. Koenig, R.D. Brown, Field-cycling relaxometry of protein solutions and tissue: Implications for MRI, Progress in Nuclear Magnetic Resonance Spectroscopy. 22 (1990) 487–567. https://doi.org/10.1016/0079-6565(90)80008-6.
[53] A. Schlüter, A. Weiss, Nuclear magnetic resonance relaxation titration, Fresenius' Zeitschrift Für Analytische Chemie. 266 (1973) 177–186.
[54] A. Schlüter, A. Weiss, Nuclear magnetic relaxation rate as indicator in complexiметric titrations, Analytica Chimica Acta. 99 (1978) 157–166.
[55] A. Schlüter, A. Weiss, Nuclear magnetic relaxation titration of Cu2+, Ni2+, Mn2+, Zn2+, and Fe3+ with 1, 10-phenanthroline hydrochloride in the presence of thiocyanate, Analytica Chimica Acta. 97 (1978) 93–110.
[56] P.F. Cobra, B.F. Gomes, C.I.N. Mitre, L.L. Barbosa, L.V. Marconcini, L.A. Colnago, Measuring the solubility product constant of paramagnetic cations using time-domain nuclear magnetic resonance relaxometry, Microchemical Journal. 121 (2015) 14–17. https://doi.org/10.1016/j.microc.2015.02.002.
[57] B.F. Gomes, J.S. da S. Burato, C.M. Silva Lobo, L.A. Colnago, Use of the Relaxometry Technique for Quantification of Paramagnetic Ions in Aqueous Solutions and a Comparison with Other Analytical Methods, International Journal of Analytical Chemistry. 2016 (2016) 1–5. https://doi.org/10.1155/2016/8256437.
[58] J. Sherwood, K. Lovas, Y. Bao, Development of an iron quantification method using nuclear magnetic resonance relaxometry, AIP Advances. 7 (2017) 056728. https://doi.org/10.1063/1.4977889.
[59] F.V.C. Kock, M.P. Machado, G.P.B. Athayde, L.A. Colnago, L.L. Barbosa, Quantification of paramagnetic ions in solution using time domain NMR. PROS and CONS to optical emission spectrometry method, Microchemical Journal. 137 (2018) 204–207. https://doi.org/10.1016/j.microc.2017.10.013.
[60] I. Solomon, Relaxation Processes in a System of Two Spins, Physical Review. 99 (1955) 559–565. https://doi.org/10.1103/PhysRev.99.559.
[61] N. Bloembergen, L.O. Morgan, Proton Relaxation Times in Paramagnetic Solutions. Effects of Electron Spin Relaxation, The Journal of Chemical Physics. 34 (1961) 842–850. https://doi.org/10.1063/1.1731684.

[62] I. Bertini, C. Luchinat, G. Parigi, 1H NMRD profiles of paramagnetic complexes and metalloproteins, in: Advances in Inorganic Chemistry, Elsevier, 2005: pp. 105–172. https://doi.org/10.1016/S0898-8838(05)57003-X.
[63] A.J. Pell, G. Pintacuda, C.P. Grey, Paramagnetic NMR in solution and the solid state, Progress in Nuclear Magnetic Resonance Spectroscopy. (2018). https://doi.org/10.1016/j.pnmrs.2018.05.001.
[64] S.H. Koenig, R.D. Brown, Relaxation of solvent protons by paramagnetic ions and its dependence on magnetic field and chemical environment: implications for NMR imaging, Magnetic Resonance in Medicine. 1 (1984) 478–495. https://doi.org/10.1002/mrm.1910010407.
[65] I. Bertini, M. Fragai, C. Luchinat, G. Parigi, Solvent 1H NMRD Study of Hexaaquochromium(III): Inferences on Hydration and Electron Relaxation, Inorganic Chemistry. 40 (2001) 4030–4035.
[66] L. Banci, I. Bertini, C. Luchinat, 1H NMRD studies of solutions of paramagnetic metal ions in ethyleneglycol, Inorganica Chimica Acta. 100 (1985) 173–181. https://doi.org/10.1016/S0020-1693(00)88305-X.
[67] I. Bertini, F. Briganti, Z. Xia, C. Luchinat, Nuclear Magnetic Relaxation Dispersion Studies of Hexaaquo Mn(II) Ions in Water-Glycerol Mixtures, Journal of Magnetic Resonance, Series A. 101 (1993) 198–201.
[68] I. Bertini, F. Capozzi, C. Luchinat, Z. Xia, Nuclear and Electron Relaxation of Fe(OH2)63+, The Journal of Physical Chemistry. 97 (1993) 1134–1137.
[69] S.H. Koenig, C. Baglin, R.D. Brown, C. Fred Brewer, Magnetic field dependence of solvent proton relaxation induced by Gd3+ and Mn2+ complexes, Magnetic Resonance in Medicine. 1 (1984) 496–501. https://doi.org/10.1002/mrm.1910010408.
[70] J. Kowalewski, A. Egorov, D. Kruk, A. Laaksonen, S. Nikkhou Aski, G. Parigi, P.-O. Westlund, Extensive NMRD studies of Ni(II) salt solutions in water and water–glycerol mixtures, Journal of Magnetic Resonance. 195 (2008) 103–111. https://doi.org/10.1016/j.jmr.2008.08.011.
[71] P.L. Anelli, I. Bertini, M. Fragai, L. Lattuada, C. Luchinat, G. Parigi, Sulfonamide-Functionalized Gadolinium DTPA Complexes as Possible Contrast Agents for MRI: A Relaxometric Investigation, European Journal of Inorganic Chemistry. 2000 (2000) 625–630. https://doi.org/10.1002/(SICI)1099-0682(200004)2000:4<625::AID-EJIC625>3.0.CO;2-2.
[72] P. Caravan, G. Parigi, J.M. Chasse, N.J. Cloutier, J.J. Ellison, R.B. Lauffer, C. Luchinat, S.A. McDermid, M. Spiller, T.J. McMurry, Albumin Binding, Relaxivity, and Water Exchange Kinetics of the Diastereoisomers of MS-325, a Gadolinium(III)-Based Magnetic Resonance Angiography Contrast Agent, Inorganic Chemistry. 46 (2007) 6632–6639. https://doi.org/10.1021/ic700686k.
[73] D.J. Mastarone, V.S.R. Harrison, A.L. Eckermann, G. Parigi, C. Luchinat, T.J. Meade, A Modular System for the Synthesis of Multiplexed Magnetic Resonance Probes, Journal of the American Chemical Society. 133 (2011) 5329–5337. https://doi.org/10.1021/ja1099616.
[74] M.W. Rotz, K.S.B. Culver, G. Parigi, K.W. MacRenaris, C. Luchinat, T.W. Odom, T.J. Meade, High Relaxivity Gd(III)–DNA Gold Nanostars: Investigation of Shape Effects on Proton Relaxation, ACS Nano. 9 (2015) 3385–3396. https://doi.org/10.1021/nn5070953.
[75] I. Bertini, O. Galas, C. Luchinat, L. Messori, G. Parigi, A theoretical analysis of the 1H nuclear magnetic relaxation dispersion profiles of diferric transferrin, The Journal of Physical Chemistry. 99 (1995) 14217–14222. https://doi.org/10.1021/j100039a006.
[76] I. Bertini, C. Luchinat, K. Nerinovski, G. Parigi, M. Cross, Z. Xiao, A.G. Wedd, Application of NMRD to Hydration of Rubredoxin and a Variant Containing a (Cys-S)3FeIII(OH) Site, Biophysical Journal. 84 (2003) 545–551. https://doi.org/10.1016/S0006-3495(03)74873-5.
[77] C. Luchinat, G. Parigi, E. Ravera, Can metal ion complexes be used as polarizing agents for solution DNP? A theoretical discussion, Journal of Biomolecular NMR. 58 (2014) 239–249. https://doi.org/10.1007/s10858-013-9728-8.

[78] S. Aime, M. Botta, E. Terreno, Gd(III)-based contrast agent for MRI, in: Advances in Inorganic Chemistry, Elsevier, 2005: pp. 173–237. https://doi.org/10.1016/S0898-8838(05)57004-1.
[79] B. Drahoš, M. Pniok, J. Havlíčková, J. Kotek, I. Císařová, P. Hermann, I. Lukeš, É. Tóth, Mn2+ complexes of 1-oxa-4,7-diazacyclononane based ligands with acetic, phosphonic and phosphinic acid pendant arms: Stability and relaxation studies, Dalton Transactions. 40 (2011) 10131. https://doi.org/10.1039/c1dt10543d.
[80] W. Nordhøy, H.W. Anthonsen, M. Bruvold, P. Jynge, J. Krane, H. Brurok, Manganese ions as intracellular contrast agents: proton relaxation and calcium interactions in rat myocardium: MANGANESE IN CARDIAC MRI, NMR in Biomedicine. 16 (2003) 82–95. https://doi.org/10.1002/nbm.817.
[81] I. Mitreiter, S.E. Oswald, F. Stallmach, Investigation of iron (III)-release in the pore water of natural sands by NMR relaxometry, The Open Magnetic Resonance Journal. 3 (2010) 46–51.
[82] R.A. Bernheim, T.H. Brown, H.S. Gutowsky, D.E. Woessner, Temperature Dependence of Proton Relaxation Times in Aqueous Solutions of Paramagnetic Ions, The Journal of Chemical Physics. 30 (1959) 950–956. https://doi.org/10.1063/1.1730133.
[83] H.G. Hertz, M. Holz, Longitudinal proton relaxation rates in aqueous Ni2+ solutions as a function of the temperature, frequency, and pH Value, Journal of Magnetic Resonance (1969). 63 (1985) 64–73. https://doi.org/10.1016/0022-2364(85)90153-2.
[84] J. Kowalewski, T. Larsson, P.-O. Westlund, Proton spin-lattice relaxation in aqueous solution of the nickel(II) ion, Journal of Magnetic Resonance (1969). 74 (1987) 56–65. https://doi.org/10.1016/0022-2364(87)90078-3.
[85] J.C. Gore, Y.S. Kang, Measurement of radiation dose distributions by nuclear magnetic resonance (NMR) imaging, Physics in Medicine and Biology. 29 (1984) 1189–1197. https://doi.org/10.1088/0031-9155/29/10/002.
[86] A. Assifaoui, personal communication, (n.d.).
[87] A.W. Nolle, L.O. Morgan, Frequency Dependence of Proton Spin Relaxation in Aqueous Solutions of Paramagnetic Ions, The Journal of Chemical Physics. 26 (1957) 642–648. https://doi.org/10.1063/1.1743361.
[88] R.J. Elias, A.L. Waterhouse, Controlling the Fenton Reaction in Wine, Journal of Agricultural and Food Chemistry. 58 (2010) 1699–1707. https://doi.org/10.1021/jf903127r.
[89] J.C. Danilewicz, Reactions Involving Iron in Mediating Catechol Oxidation in Model Wine, American Journal of Enology and Viticulture. 64 (2013) 316–324. https://doi.org/10.5344/ajev.2013.12137.
[90] J.C. Danilewicz, Role of Tartaric and Malic Acids in Wine Oxidation, Journal of Agricultural and Food Chemistry. 62 (2014) 5149–5155. https://doi.org/10.1021/jf5007402.
[91] G.Y. Kreitman, J.C. Danilewicz, David.W. Jeffery, R.J. Elias, Reaction Mechanisms of Metals with Hydrogen Sulfide and Thiols in Model Wine. Part 2: Iron- and Copper-Catalyzed Oxidation, Journal of Agricultural and Food Chemistry. 64 (2016) 4105–4113. https://doi.org/10.1021/acs.jafc.6b00642.
[92] C. Roullier-Gall, M. Witting, F. Moritz, R.B. Gil, D. Goffette, M. Valade, P. Schmitt-Kopplin, R.D. Gougeon, Natural oxygenation of Champagne wine during ageing on lees: A metabolomics picture of hormesis, Food Chemistry. 203 (2016) 207–215. https://doi.org/10.1016/j.foodchem.2016.02.043.
[93] M. Nikolantonaki, P. Julien, C. Coelho, C. Roullier-Gall, J. Ballester, P. Schmitt-Kopplin, R.D. Gougeon, Impact of Glutathione on Wines Oxidative Stability: A Combined Sensory and Metabolomic Study, Frontiers in Chemistry. 6 (2018). https://doi.org/10.3389/fchem.2018.00182.
[94] C. Coelho, P. Julien, M. Nikolantonaki, L. Noret, M. Magne, J. Ballester, R.D. Gougeon, Molecular and Macromolecular Changes in Bottle-Aged White Wines Reflect Oxidative

Evolution–Impact of Must Clarification and Bottle Closure, Frontiers in Chemistry. 6 (2018). https://doi.org/10.3389/fchem.2018.00095.
[95] C. Roullier-Gall, B. Kanawati, D. Hemmler, G.K. Druschel, R.D. Gougeon, P. Schmitt-Kopplin, Electrochemical triggering of the Chardonnay wine metabolome, Food Chemistry. 286 (2019) 64–70. https://doi.org/10.1016/j.foodchem.2019.01.149.
[96] J.C. Danilewicz, P. Tunbridge, P.A. Kilmartin, Wine Reduction Potentials: Are These Measured Values Really Reduction Potentials?, Journal of Agricultural and Food Chemistry. 67 (2019) 4145–4153. https://doi.org/10.1021/acs.jafc.9b00127.
[97] E.V. Goldammer, M.D. Zeidler, Molecular motion in aqueous mixtures with organic liquids by nmr relaxation measurements, Berichte Der Bunsengesellschaft Für Physikalische Chemie. 73 (1969) 4–15. https://doi.org/10.1002/bbpc.19690730105.
[98] P. Pohl, B. Prusisz, Chemical fractionation of Cu, Fe and Mn in canned Polish beers, Journal of Food Composition and Analysis. 23 (2010) 86–94. https://doi.org/10.1016/j.jfca.2009.08.002.
[99] A.M. Green, G.R. Scollary, Influence of metal ions on lead complexation in wine, Australian Journal of Grape and Wine Research. 6 (2000) 197–202. https://doi.org/10.1111/j.1755-0238.2000.tb00179.x.

Figure captions

Fig. 1.

NMRD profiles of real and model wines. Black and pink symbols represent profiles of real wine (Wa, Ra, ○; Rb, ○) and exchanged wine (EW, ●). Blue symbols report profile of synthetic wine MW005 (50µg/L Mn^{2+}) and MW128 (1.28 mg/L Mn^{2+}). Continuous lines result from the refinement of real and model wines, individual components of the fits are represented by dashed lines. (a) white wine Wa with MW005 and MW128. (b) vertical extension of the profile of MW005 with its refinement and related components along with the EW profile. (c) Red wines, with Ra refinement of. The profile of Wb overlaps Wa one's and is not reported.

to the Wa one and is not reported.

Fig. 2.

Variation of C_C, and C_D parameters for the model wines.

Fig. 3.

Proton relaxivity of model wines versus metal concentration, recorded at 19.65 MHz. Continuous lines correspond to linear regressions. For linear regressions of model wines containing Ni^{2+}, Cu^{2+}, and Fe^{2+} relaxation times of wines with 50, 25 and10 mg/L have been measured (data not shown).

Fig. 4.

Relaxation rate of alcoholic solutions, (●) Hydro-alcoholic solution, (○) alcoholic solution with 1.2 mg/L of Mn^{2+}, and (▲)alcoholic solution containing 1.23 mg/L of manganese and 5g/L of tartaric acid, versus the alcohol percent in volume (alc/vol) at 25 °C.

Fig. 5.

Manganese concentration calculated on MW053. Only half of the symmetrical data is plotted. Color legend is expressed in mg/L and contour plot levels are drawn every 0.05 mg/L. Square, dashed rectangle and triangle are arbitrary zones for statistical calculations. No processing of the data (filtering, smoothing, or interpolation) is applied.

Fig. 6.

Manganese concentration calculated on Wa. Color legend is expressed in mg/L and levels are uniformly represented with a 0.15 mg/L step. Square, rectangle and triangle are calculation zones consistent with Fig. 6. No data processing is applied.

Fig. 1

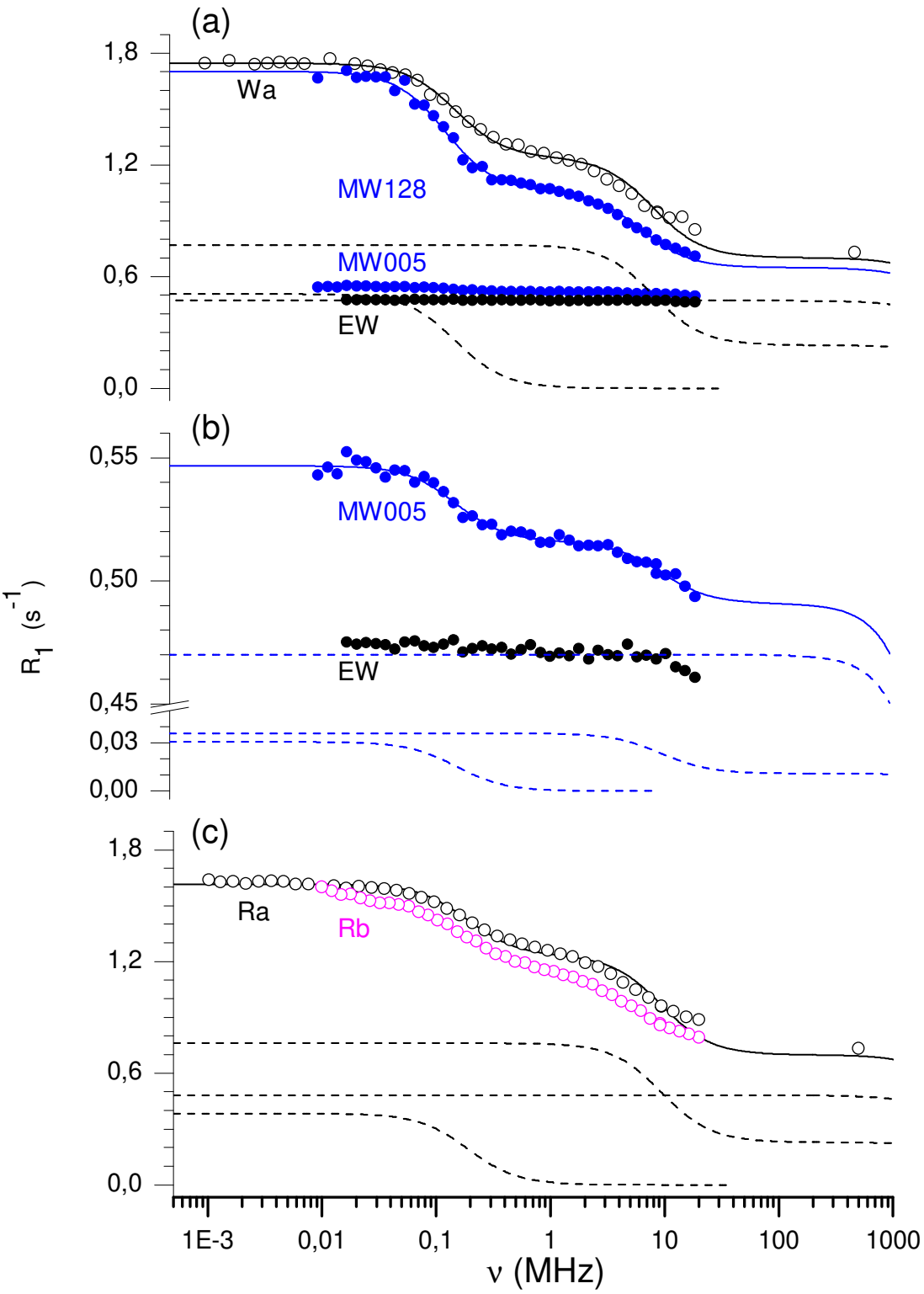
(a)
1,8
1,2
0,6
0,0
Wa
MW128
MW005
EW
(b)
0,55
0,50
0,45
0,03
0,00
MW005
EW
(c)
1,8
1,2
0,6
0,0
Ra
Rb
1E-3
0,01
0,1
1
10
100
1000
ν (MHz)
R1 (s-1)

Fig. 2.

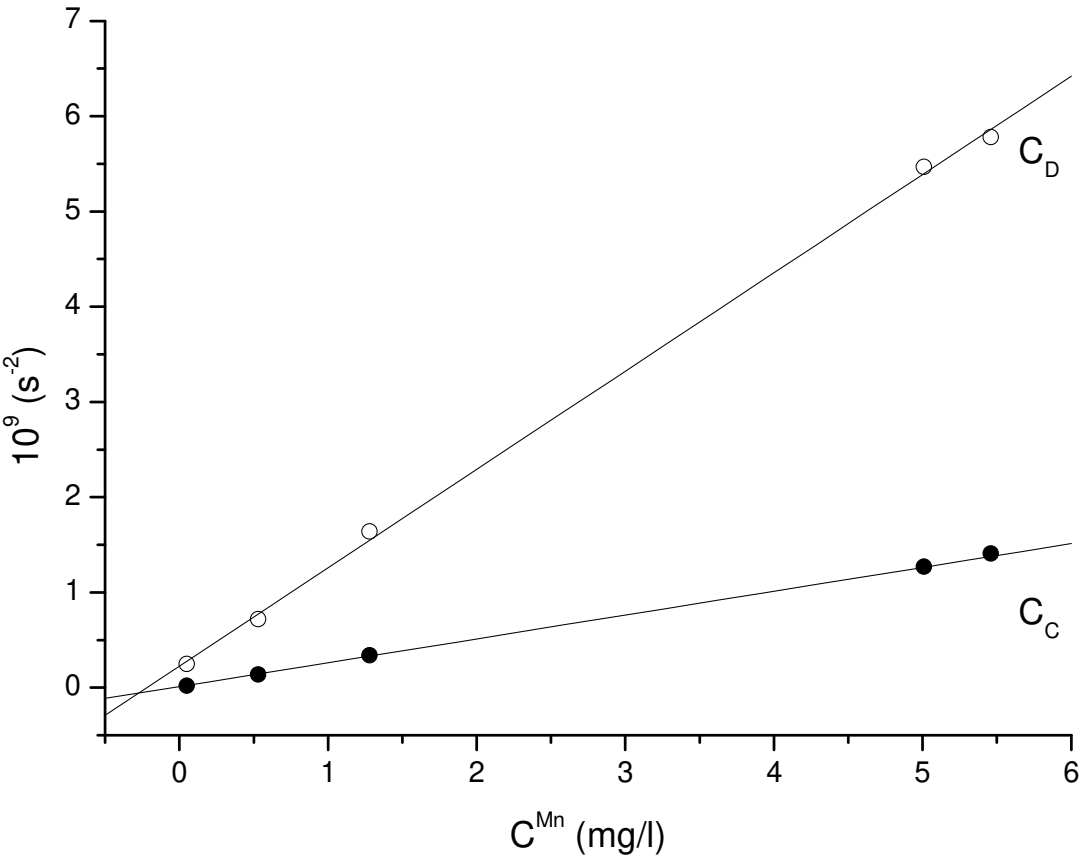

Fig. 3.

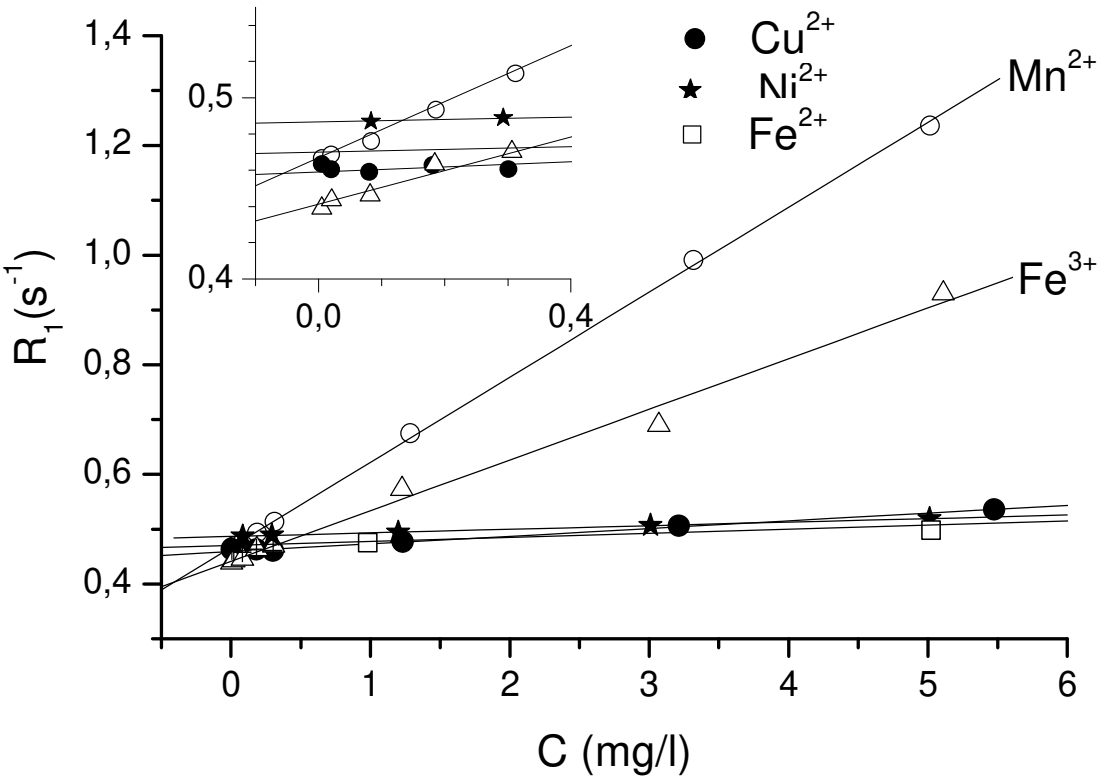
1,4
1,2
1,0
0,8
0,6
0,4
0,5
0,4
0,0
0,4
$R_1(s^{-1})$
Cu^{2+}
Ni^{2+}
Fe^{2+}
Mn^{2+}
Fe^{3+}
0
1
2
3
4
5
6
C (mg/l)

Fig. 4.

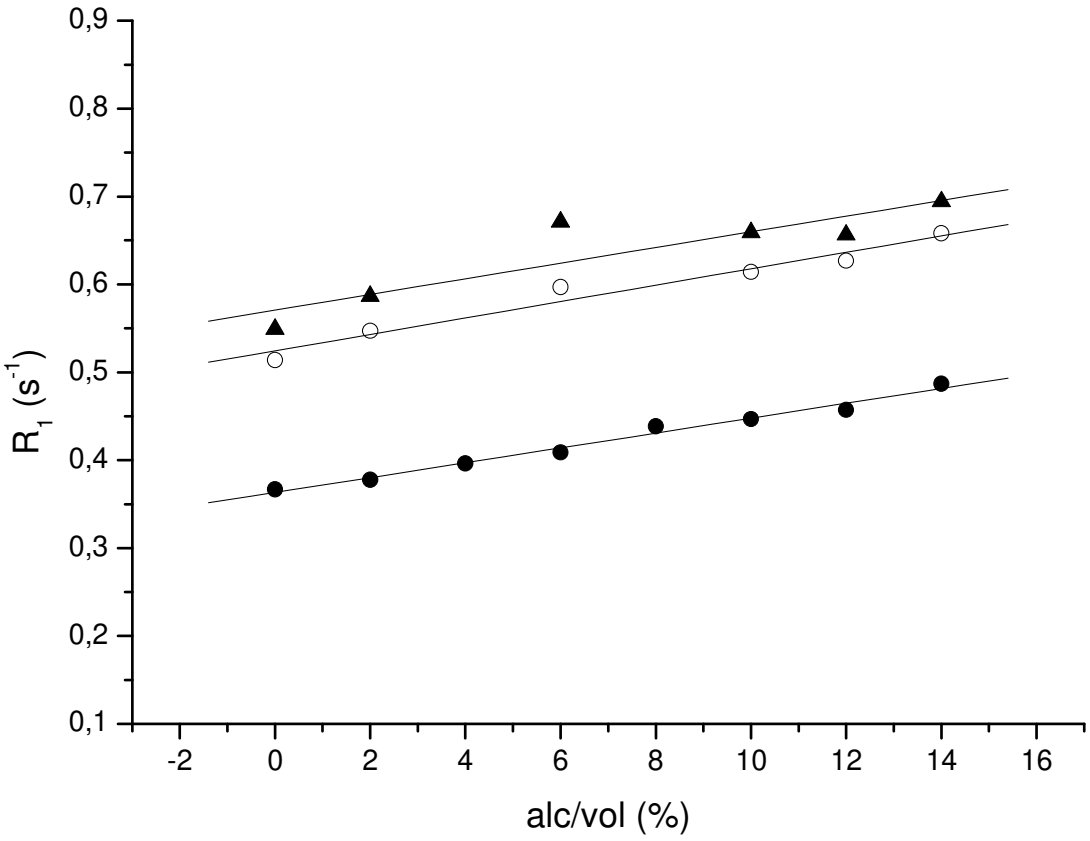

Fig. 6.

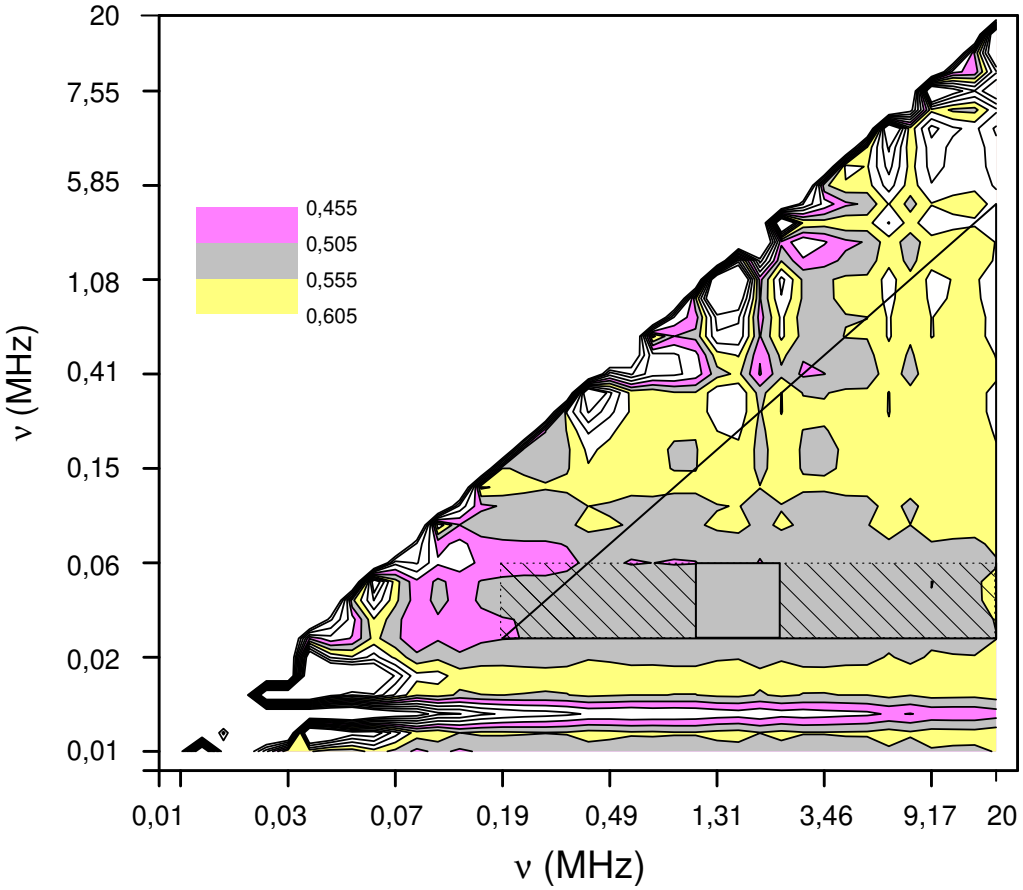
20
7,55
5,85
1,08
0,41
0,15
0,06
0,02
0,01
ν (MHz)
0,455
0,505
0,555
0,605
0,01
0,03
0,07
0,19
0,49
1,31
3,46
9,17
20
ν (MHz)

Fig. 7.

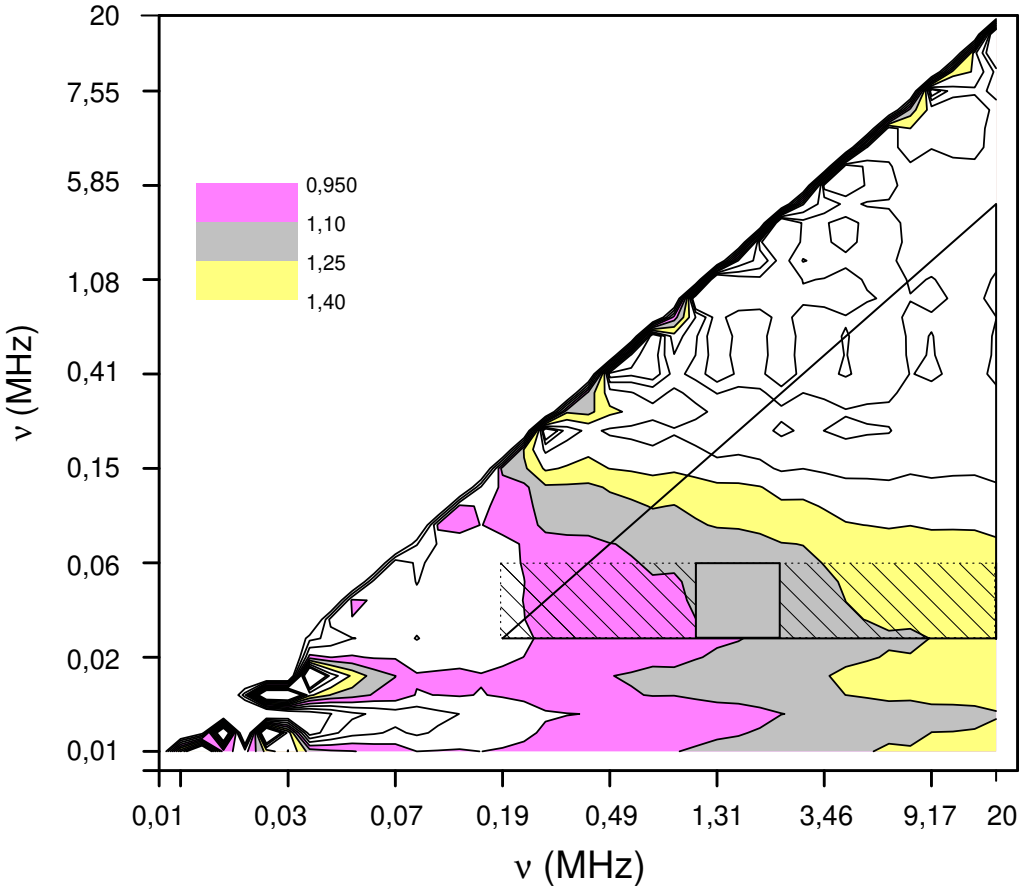
20
7,55
5,85
1,08
0,41
0,15
0,06
0,02
0,01
ν (MHz)
0,950
1,10
1,25
1,40
0,01
0,03
0,07
0,19
0,49
1,31
3,46
9,17
20
ν (MHz)

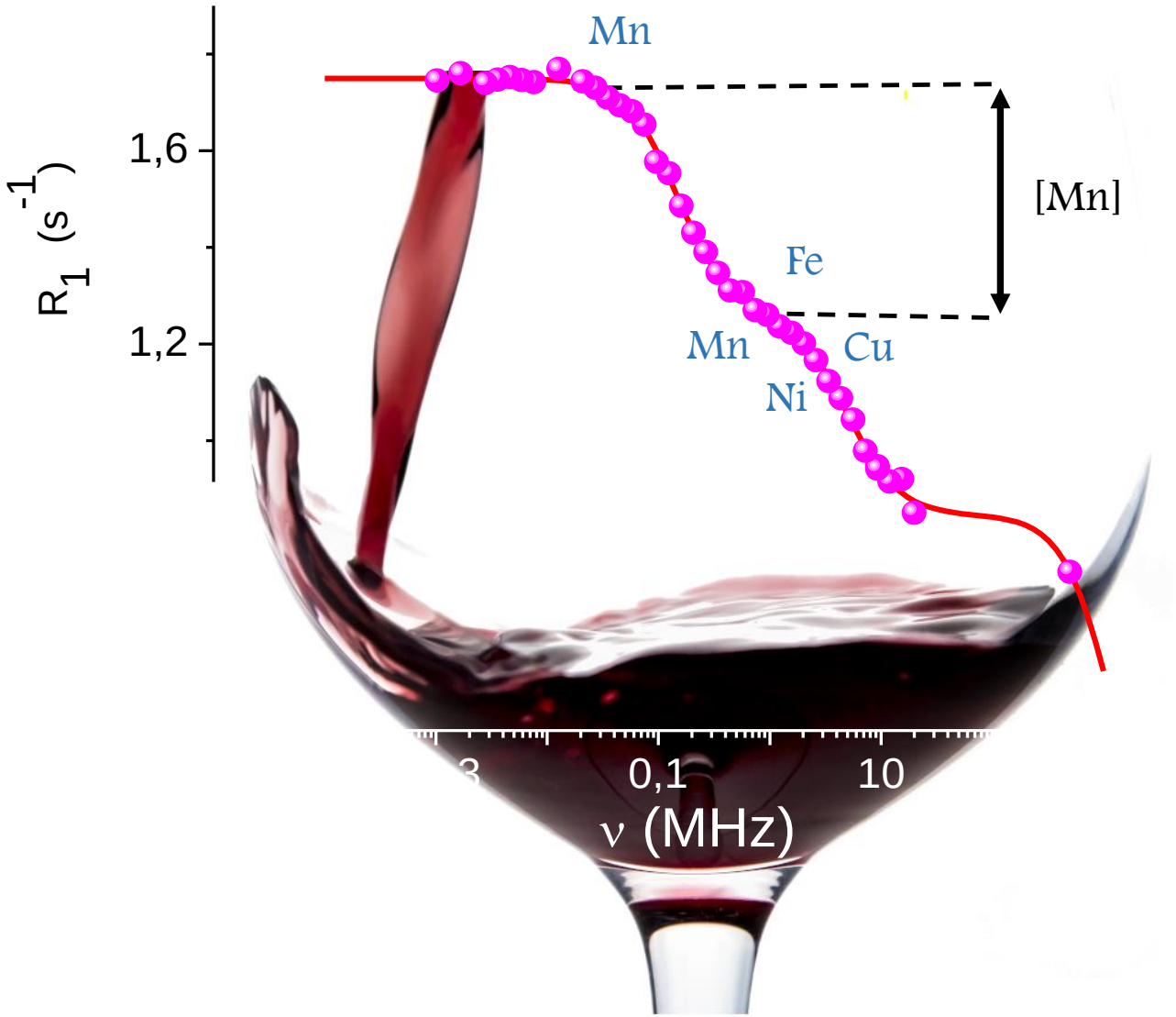
Mn
Fe
Mn
Cu
Ni
[Mn]
1,6
1,2
R_1 (s^{-1})
3
0,1
10
ν (MHz)